ACS APPLIED MATERIALS & INTERFACES

Letter

Cite This: ACS Appl. Mater. Interfaces 2018, 10, 2230−2235

www.acsami.org

Atomic-Scale Insights into the Oxidation of Aluminum

Lan Nguyen,[†] Teruo Hashimoto,[†] Dmitri N. Zakharov,[‡] Eric A. Stach,[‡,§,⊥] Aidan P. Rooney,[†] Benjamin Berkels,[∥] George E. Thompson,[†] Sarah J. Haigh,[*,†] and Tim L. Burnett[*,†]

[†]School of Materials, University of Manchester, Oxford Road, Manchester M13 9PL, United Kingdom

[‡]Center for Functional Nanomaterials, Brookhaven National Laboratory, Upton, New York 11973, United States

[§]University of Pennsylvania, Laboratory for Research on the Structure of Matter, 3231 Walnut Street, Philadelphia, Pennsylvania 191041, United States

[∥]Department of Mathematics, RWTH Aachen University, Schinkelstrasse 2, 52062 Aachen, Germany

Supporting Information

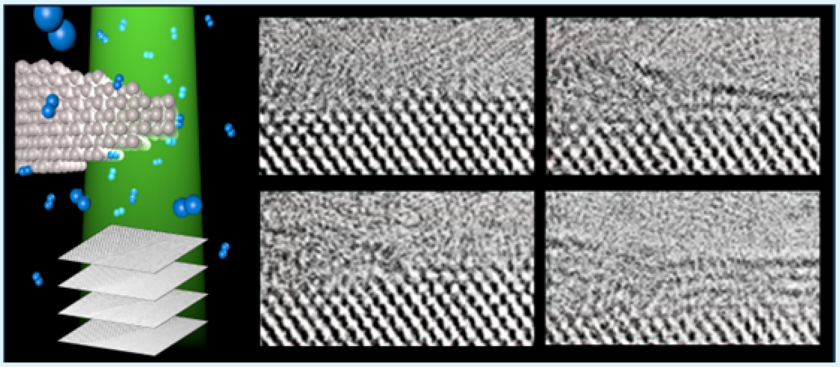

ABSTRACT: The surface oxidation of aluminum is still poorly understood despite its vital role as an insulator in electronics, in aluminum−air batteries, and in protecting the metal against corrosion. Here we use atomic resolution imaging in an environmental transmission electron microscope (TEM) to investigate the mechanism of aluminum oxide formation. Harnessing electron beam sputtering we prepare a pristine, oxide-free metal surface in the TEM. This allows us to study, as a function of crystallographic orientation and oxygen gas pressure, the full oxide growth regime from the first oxide nucleation to a complete saturated, few-nanometers-thick surface film.

KEYWORDS: *oxide, nucleation, transmission electron microscopy, aluminum, high resolution transmission electron microscopy, environmental transmission electron microscopy, electron energy loss spectroscopy*

INTRODUCTION

The ability of aluminum to spontaneously form a self-healing surface oxide is crucial for the metal's function in a broad range of applications, yet the full oxide formation process remains poorly understood. The early stages of oxygen molecule absorption have been effectively elucidated via surface science techniques (such as scanning tunneling microscopy),[1,2] whereas the overall growth kinetics have been widely studied with macroscopically averaging surface characterization techniques such as X-ray photoemission spectroscopy (XPS).[3−5] In contrast, the intermediate stages of oxide development, including the mechanism of oxide nucleation and growth remains elusive due to the lack of atomically resolved techniques able to directly observe dynamic atomic rearrangements for increasing oxide thicknesses at relevant pressures. This is a significant challenge as the reactivity of aluminum means that in situ preparation and high vacuum are required to maintain a pristine substrate. In addition, the stable native oxide that forms on aluminum is difficult to remove by reduction[6] especially when dealing with delicate samples. In this work, we demonstrate how state-of-the-art atomic resolution aberration corrected environmental transmission electron microscope (E-TEM)[7] imaging can address this knowledge gap.

High-resolution electron microscopy studies of aluminum oxidation are often hindered by the difficulty of preparing a pristine metal specimen due to aluminum's high reactivity with trace oxygen. Additionally, the high stability of aluminum oxide[8] makes it slow to remove using gas-based reduction methods in the E-TEM, although other metals like Cu[9,10] and Ni[11,12] have proved amenable to this specimen preparation approach. Here we show that it is possible to prepare pristine aluminum metal surfaces in the TEM by condensing the electron beam to produce a high local electron flux. This removes the native oxide via electron beam sputtering. Particular crystallographic surfaces can be prepared in this way allowing a comparison of their different oxidation behavior as a function of oxygen pressure. Our results demonstrate how the E-TEM can bridge the gap between surface

Received: November 12, 2017
Accepted: January 2, 2018
Published: January 10, 2018

DOI: 10.1021/acsami.7b17224
ACS Appl. Mater. Interfaces 2018, 10, 2230−2235

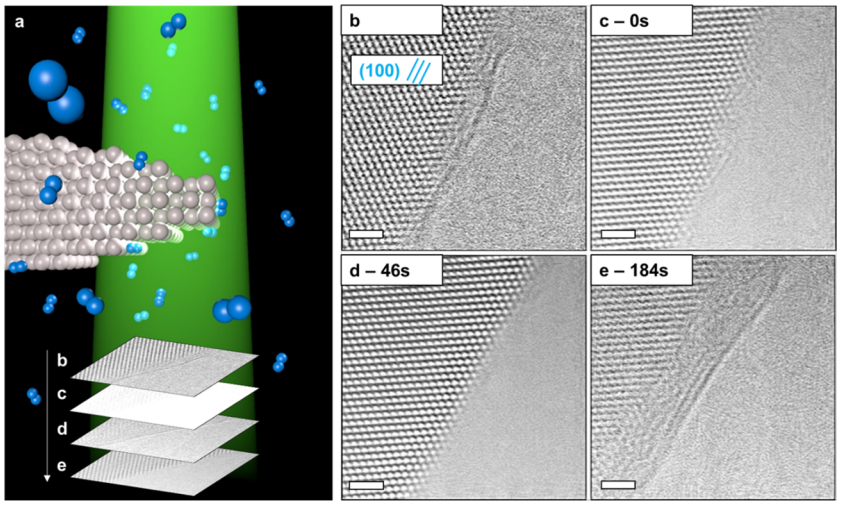

Figure 1. (a) Artist's illustration showing environmental TEM imaging of an aluminum specimen in an O_2 gas environment (green = electrons; blue = oxygen; gray = aluminum). Times stated are from the point of oxygen introduction shown in c (full sequence: SV1). (b–d) Sequential atomic resolution images of Al sample viewed down the [011] zone axis direction with an exposed (100) surface facet parallel to the electron beam. (b) Shows evidence of the presence of the initial oxide formed before loading the sample in the TEM. This had already been partially sputtered away due to the high electron flux >54 000 e $Å^{-2}$ s^{-1} so the observed oxide thickness is not representative of the initial oxide shown in Figure S2. (c) Once the oxide film has been fully removed the surface is atomically pristine aluminum. (d) 46 s and (e) 184 s after oxygen gas was introduced, the regrowth of aluminum's self-healing surface oxide is measured in situ. Scale bar in b–e: 1 nm.

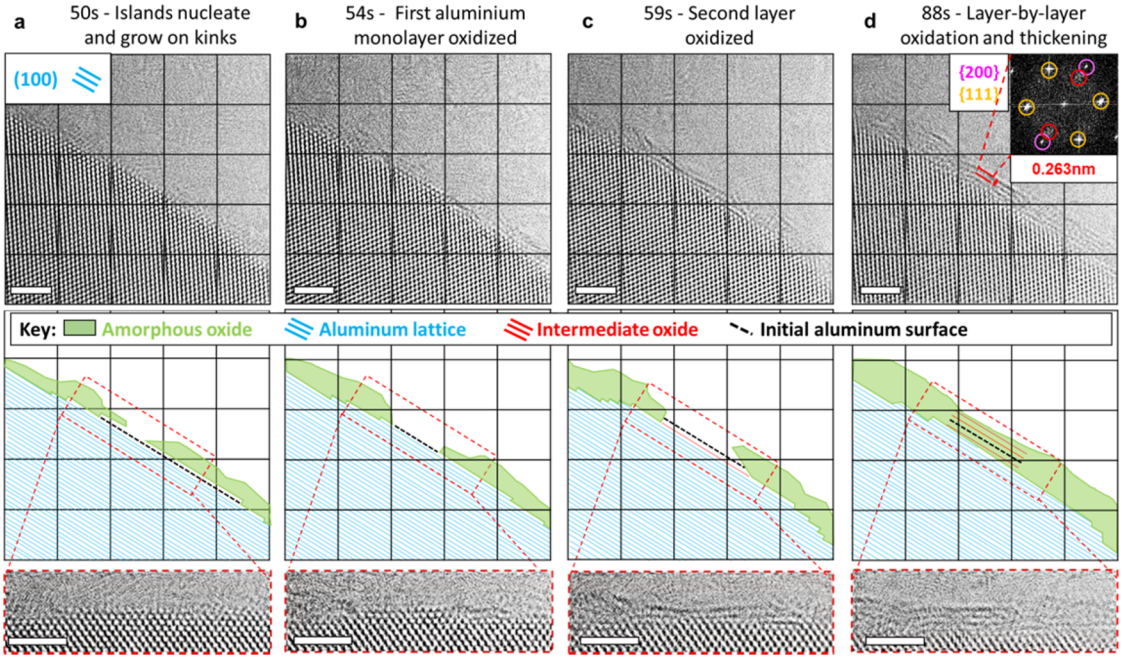

Figure 2. (a–d) Top: Time-resolved E-TEM images showing key points during layer-by-layer oxidation and oxide growth from an atomically pristine Al (100) surface facet. Times stated are after oxygen introduction. The full growth sequence can be seen in Video SV1. Bottom: schematic illustrations of the structures visible in the top TEM images, with enlarged TEM image of the surface region shown below. A 5 × 5 array of gridlines is used to guide the eye between experimental image and schematic. (a) First islands nucleate on atomic kinks. Black dashed line shows location of original metal-oxide interface. (b) Islands grow until the first atomic layer between islands becomes amorphous oxide. (c, d) Growth proceeds layer-by-layer until a continuous oxide is formed. The solid–gas interface has moved due to oxygen incorporation from the gas. The FT of d is shown enlarged and inset, with red circles highlighting the lattice spacing of the intermediate surface oxide (0.263 nm) epitaxial to the native aluminum surface (aluminum (200) lattice spacing highlighted by purple circles). Aluminum is viewed down Al [011] zone axis direction (T = 273 K, pressure: 3×10^{-5} Torr). All scale bars: 2 nm.

science techniques and bulk characterization, allowing direct linking of atomic scale mechanisms with the macroscopic growth behavior to better understand the oxide formation on aluminum. We envisage that the approach demonstrated in this work, creating atomically clean facets and then observing their reoxidation in E-TEM, should be a transferrable method to study the nucleation and growth mechanisms to near-saturation thicknesses for many spontaneously forming surface oxides.

Figure 1a, shows a schematic of the E-TEM imaging of an aluminum specimen, prepared by ultramicrotomy, in an oxygen gas environment. High-resolution TEM image sequences (Figure 1b–d) demonstrate the removal of the native surface

DOI: 10.1021/acsami.7b17224
ACS Appl. Mater. Interfaces 2018, 10, 2230–2235

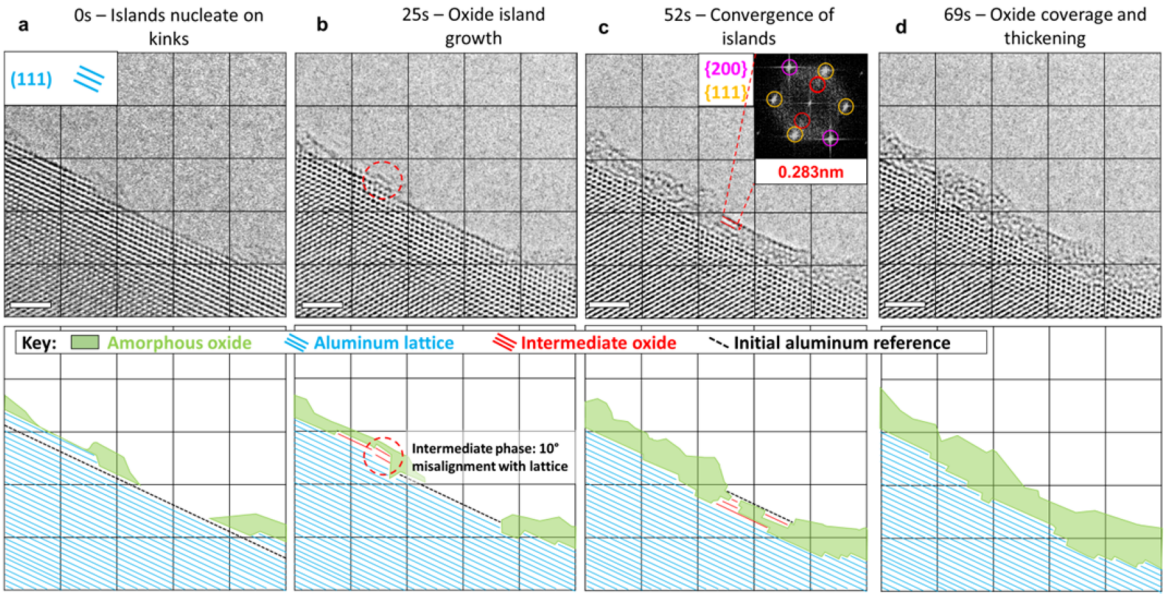

Figure 3. (a–d) Top: Time-resolved E-TEM images showing layer-by-layer oxidation and oxide growth from an atomically pristine Al (111) facet. Times stated are from the point of oxygen introduction which is also the start of the full image sequence (120 s) shown in Video SV2. Bottom: schematic illustrations of the different structures visible in the TEM images. A 5 × 5 array of gridlines is used to guide the eye between experimental image and schematic. (a) Nucleation of oxide islands at lattice kinks. Black dashed line shows location of original metal-oxide interface. (b) Development of the oxide islands producing a spalled intermediate phase within the developing oxide (rotated 10° with respect to (200) planes of native aluminum lattice). (c) Formation of a neck region between islands revealing an unexpected lateral growth mode. Intermediate phase formed has a lattice spacing of 0.283 nm. (d) Uniform coverage of oxide is achieved after which the oxide thickens slowly. All scale bars: 2 nm.

oxide to prepare a pristine metal surface on which to study oxide formation. We observe that in high vacuum conditions (3×10^{-7} Torr), a high flux (greater than 54 000 e $Å^{-2}$ s^{-1} for 5–10 s), sputters atoms from the material leaving a clean faceted metal surface.[13,14] The high current density of the condensed beam and the electrically insulating nature of the aluminum oxide can also produce electrostatic charging, which may further contribute to the substantial collective mass loss from the surface.[13−16] As well as the loss of native oxide we also observe a tendency for surface faceting, likely due to the rearrangement of atomic terraces to minimize surface energy (see Figure S1 for faceting of Al(100) following oxide removal). The ability to simply and reliably produce clean faceted metal surfaces with which to study oxidation in the TEM is likely to be a key tool for future E-TEM investigations.

Figure 2 shows key steps in the oxidation of a (100) surface facet at an oxygen pressure of 3×10^{-5} Torr. Figure 2a shows the early stage of oxidation where oxide islands nucleate at atomic terraces on the surface, which act as high surface energy heterogeneous nucleation sites where oxygen can preferentially adsorb.[17−19] The oxide islands are then observed to grow laterally toward one another (Figure 2b, c). Lateral island growth has previously been observed for copper oxidation by in situ TEM and is believed to occur via surface diffusion of oxygen species and preferential adsorption on surface sites at the edges of islands.[17−20] The pristine aluminum facet remains clean, most likely because adjacent oxide islands act as "sinks" for reacting species which diffuse across the surface. Aluminum terraces on the surface are consumed by reactants diffusing to the growth front.[17,19] The majority of theoretical models for aluminum oxidation assume a uniform vertical growth front and our results demonstrate that this is not applicable to the earliest stages of oxidation.[21]

Figure 2b shows that as the oxide islands continue to grow, a single atomic plane of aluminum appears to oxidize at the surface between two islands, visible as a loss of image contrast and ordering. Soon afterward, a second layer of the surface also loses contrast, suggesting that oxidation then proceeds layer-by-atomic-layer into the aluminum. After sufficient time a continuous semicrystalline layer of oxide ∼1.5 nm thick, covers the surface (Figure 2d), which is close to the saturation thickness measured by XPS for aluminum at comparable pressures but higher temperature.[4,22] The oxide region appears to retain some crystalline order, aligned with respect to the aluminum surface but with increased lattice spacing. The number of atomic planes of these ordered oxide regions corresponds directly to the number of aluminum surface planes transformed from the aluminum lattice (see Video SV1). The inset Fourier transform (FT) in Figure 2d shows the spacing of this intermediate oxide is ∼0.263 ± 0.1 nm, which is around a 30% expansion from the Al(200) spacing of 0.203 nm. Many previous studies have reported the formation of an intermediate γ-Al_2O_3 phase, which grows with commensurate structure to the parent aluminum lattice.[4,5,20,23] However, a detailed structural identification remains elusive, and the structure and stoichiometry of this γ-Al_2O_3 intermediate is controversial; likely due to strong dependency on oxide growth conditions and the fact that the intermediate phase forms on the nanoscale.[24] The increased spacing of the intermediate oxide phase relative to pure aluminum is likely due to oxygen incorporation into the aluminum lattice. The presence of an unidentified aluminum oxide phase is not unexpected; γ-Al_2O_3 is known to show large structural differences due to variations in stoichiometry, temperature, pressure, and film thickness.[24,25] The fully thickened film shows no long-range crystallinity, consistent with the expected amorphous oxide structure (see Video SV1).

DOI: 10.1021/acsami.7b17224
ACS Appl. Mater. Interfaces 2018, 10, 2230−2235

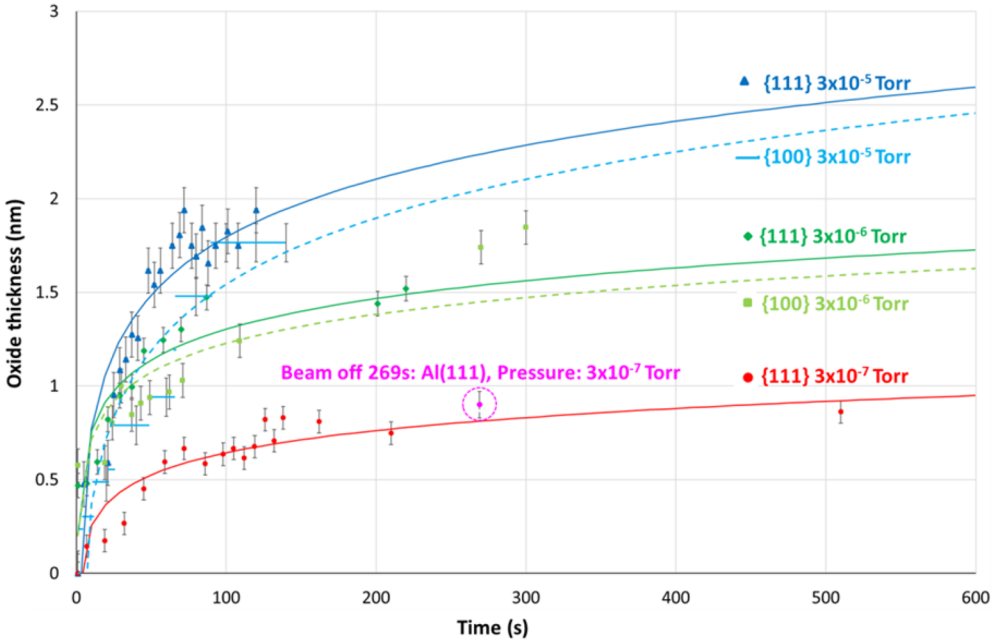

Figure 4. Kinetics of oxidation for[27] and {100} surface facets of aluminum at oxygen pressures of: 3×10^{-5}, 3×10^{-6}, and 3×10^{-7} Torr. Oxide thickness measurements are fit to logarithmic trend lines representing growth of oxides to critical thickness according to the Cabrera−Mott theory. Higher pressures show faster initial rates of oxidation and lead to oxide films of larger critical thickness. The encircled point at 269 s (0.9 nm thickness) is the control experiment where the beam was blanked for Al(111) at a pressure of 3×10^{-7} Torr. The growth observed without electron beam irradiation is comparable to the same oxidation conditions acquired with continuous electron beam observation (red line, Al(111) at pressure of 3×10^{-7} Torr, electron flux of 11 000 e $Å^{-2}$ s^{-1}).

Figure 3 shows the same oxidation process, again at an oxygen pressure of 3×10^{-5} Torr, but now for a different crystallographic surface; Al(111). We observe the nucleation of oxide islands at atomic terraces (Figure 3a), followed by island growth. However, compared to the Al(100) surface, differences are observed in the process of growth. On Al(111) the oxide was observed to grow into the aluminum lattice beneath the island, with part of the aluminum surface starting to exfoliate, rotating 10° relative to the bulk. This can be explained by the high dynamic stresses that are generated in amorphous oxides due to free volume generation (compared to bulk Al(111)).[26] For partially coherent oxide-metal interfaces, high interfacial stresses may be generated in the intermediate phases due to the large mismatch in the lattice spacings for bulk aluminum and the equilibrium γ-Al_2O_3 phase (~0.310 ± 0.1 nm).[8] In some cases, oxidation occurs first along a row of atoms beneath the surface (Figure 3c), rather than the uppermost atomic plane. This forms a semicrystalline oxide bridge between two neighboring oxide islands. Convergence of aluminum oxide islands by "necking" has been observed by Jeurgens but not with this level of atomic detail.[20] The bridge region is observed to contain an intermediate oxide phase, aligned parallel to Al(111) planes but with a larger lattice spacing of 0.283 ± 0.1 nm. This lattice expansion on Al(111) (21%) is smaller than the 30% expansion seen for the Al(111) surface perhaps due to differences in the way oxygen chemisorbs to the surface. Flottoto et al. observed that stresses within amorphous oxides formed on Al(111) facets are considerably higher than for Al(100).[26] They speculated that this was because oxygen chemisorbed on the close-packed (111) planes forms an ordered structure which hinders stress relaxation during the oxide growth process. When all the islands have coalesced the full surface is covered in an oxide film ~1.5 nm thick. After complete surface coverage the rate of oxide growth slows; the film gradually thickens and the semicrystalline intermediate oxide phases steadily amorphise completely. The full growth sequences for Al(100) and (111) surface facets are available in Videos SV1 and SV2, respectively.

Figure 4 shows the average thickness of the aluminum oxide formed on {100} and {111} surfaces as a function of oxygen pressure (3×10^{-5}, 3×10^{-6}, and 3×10^{-7} Torr). More details of measuring growth rate are shown in Figure S3. The Cabrera−Mott theory models low temperature oxidation as driven by the electric field produced by the charge separation due to the presence of metal ions at the oxide-gas interface and oxygen ions at the metal-oxide interface.[21] It predicts that oxide growth is rapid until an oxide completely covers the surface. After this the oxide film thickens at a slower rate, as a result of the increased charge separation across the growing oxide layer. All growth curves we observed follow the same general kinetic trends as predicted by the Cabrera−Mott theory (Figure 4). The differences we observe for the early stages of nucleation and growth are likely due to the unavoidable pressure gradient as gas is introduced to the column as well as local surface variations (kinks, steps, etc.) that are not included in the general theory.

The critical thickness of oxide at saturation is dependent on the oxygen pressure, with higher pressures resulting in quicker initial rates of oxidation and higher critical oxide thickness.[28] At pressures below 3×10^{-5} Torr, we observe similar island growth at surface steps to that illustrated in Figures 2 and 3 (both observed at 3×10^{-5} Torr), but at lower pressure the process occurs over longer time scales. This relationship between critical oxide thickness and oxygen pressure has been previously reported in XPS studies,[3,28,29] and is attributed to higher pressures producing a larger concentration of oxygen molecules on the surface of the metal which are available for oxidation and growth, according to Langmuir isotherm behavior.[28,29] The higher concentration of adsorbed oxygen at higher pressures also increases the oxide growth rate by increasing the electric field and

DOI: 10.1021/acsami.7b17224
ACS Appl. Mater. Interfaces 2018, 10, 2230−2235

thus the rate of ionic migration through the oxide.[29] At the lowest pressure tested (3×10^{-7} Torr), we do not observe any oxide formation even after 1 h on the Al(100) facet, although the Al(111) surface reached close to its critical thickness ~0.9 nm after 600 s. Elemental mapping of the oxide using electron energy loss spectroscopy (EELS) shows that oxides are oxygen rich at the metal-oxide interface, but that the oxygen concentration drops at the oxide−gas interface (Figure S4). The summed EELS spectrum (Figure S5) also shows that there are no surface contaminants (such as carbon) in the oxide within the limits of detectability, (locally $\lesssim$1%).

In all dynamic TEM experiments, it is important to consider the effect that imaging with the electron beam could have on the reaction being observed. To prepare the pristine metal surface we have harnessed electron beam sputtering at high electron flux ($\geq$54 000 e Å^{-2} s^{-1}) to remove the oxide. To assess the effect the electron beam could have on oxidation we have prepared the Al(100) pristine surface in the same way but performed the experiment at an oxygen pressure of 3×10^{-7} Torr "in the dark"; only imaging after 269 s. The thickness measured with the electron beam off is in good agreement with that observed for the continuously imaged surface (0.82 ± 0.1 nm compared to 0.90 ± 0.1 nm with the beam on).

Nevertheless, we note that this agreement between data obtained for beam-off and beam-on conditions is only obtained by controlling electron flux below a critical value when imaging continuously. For a flux above ~12 000 e Å^{-2} s^{-1}, we observed crystallization of the amorphous oxide films (see Videos SV3 and SV4). Previous work by Popova[30] and Zhukov[31] has observed that the later stages of aluminum oxide growth can be enhanced by an applied voltage and for 100 eV electron irradiation. Nevertheless, the good agreement we find compared to bulk thickness measurements suggests that this effect is small in our case. Our measurements of the lattice spacings of this irradiation induced oxide phase show that it has a crystal spacing of 0.240 nm for Al(111), a good match to the irradiation induced intermediate γ-Al_2O_3, oxide observed previously in oxidized aluminum.[32,33] However, it differs significantly from the intermediate oxide layers we observe during our in situ experiments, supporting our understanding that the electron beam has a negligible influence on the reaction we observe.

CONCLUSION

In conclusion, we find that the overall oxide growth behavior we observe is in good agreement with both surface science measurements of the early stages of oxidation and with average data from bulk techniques. By bridging an elusive gap between the time and length scales of these different methods, E-TEM allows observation of the full process of metal oxide growth: providing insights into the different oxidation mechanisms for different crystallographic surfaces. We reveal that oxidation of Al(100) occurs via island growth and surface oxidation, whereas for Al(111), the oxide can grow along an atomic plane below the uppermost surface layer. This has important implications for optimizing the corrosion, aesthetic and insulating properties of aluminum oxide coatings for a wide range of applications. Our control experiments demonstrate that below a critical electron flux the effect of the electron beam is negligible. However, by harnessing electron beam sputtering at high flux, we show that this E-TEM approach can be applied to study oxide nucleation even where a material spontaneously oxidizes in ambient conditions. This provides new opportunities for studying oxidation, corrosion, and phase transformations for many industrially important materials including self-passivating metallurgical systems such as magnesium and titanium, readily oxidizing catalytic nanoparticles like cobalt, and air-sensitive electrode materials.

ASSOCIATED CONTENT

Supporting Information

The Supporting Information is available free of charge on the ACS Publications website at DOI: 10.1021/acsami.7b17224.

Experimental methods, EEL spectrum imaging, unfiltered TEM images (PDF)

Video SV1 showing oxidation of Al(100) at an oxygen pressure of 3×10^{-5} Torr (variable electron flux); stills from this video are presented in the Figures 1 and 2 (AVI)

Video SV2 showing oxidation of Al(111) (SV2) at an oxygen pressure of 3×10^{-5} Torr (variable electron flux); stills from this video are presented in Figure 3 (AVI)

Video SV3 showing imaging above critical electron flux (12 000 e Å^{-2} s^{-1}) with instant recrystallization of oxide (AVI)

Video SV4 showing imaging below critical flux (11 000 e Å^{-2} s^{-1}) showing no crystallization of oxide (AVI)

AUTHOR INFORMATION

Corresponding Authors

*E-mail: sarah.haigh@manchester.ac.uk.
*E-mail: timothy.burnett@manchester.ac.uk

ORCID

Eric A. Stach: 0000-0002-3366-2153
Aidan P. Rooney: 0000-0002-1333-9359
Sarah J. Haigh: 0000-0001-5509-6706

Present Address

[⊥]Department of Materials Science and Engineering, University of Pennsylvania, 220 South 33rd Street, 107 Towne Building, Philadelphia, PA 19104-6391.

Author Contributions

L.N., S.J.H., T.H., and T.L.B. analyzed the data and G.E.T. contributed to the discussion. B.B. contributed to the data processing. L.N., T.L.B., and S.J.H. wrote the manuscript and prepared the figures. T.H., D.Z., and E.S. performed the electron microscopy experiments. A.P.R. created the 3D image used in Figure 1a. All authors have given approval to the final version of the manuscript.

Notes

The authors declare no competing financial interest.

ACKNOWLEDGMENTS

The authors thank the Engineering and Physical Sciences (EPSRC) U.K Grants EP/G035954/1, EP/K016946/1, and Defence Threat Reduction Agency Grant HDTRA1-12-1-0013 for funding. This research used resources of the Center for Functional Nanomaterials, which is a U.S. DOE Office of Science Facility, at Brookhaven National Laboratory, under Contract DE-SC0012704. S.J.H. has received funding from the European Research Council (ERC) under the European Union's Horizon 2020 research and innovation programme (grant agreement ERC-2016-STG-EvoluTEM-715502).

DOI: 10.1021/acsami.7b17224
ACS Appl. Mater. Interfaces 2018, 10, 2230−2235

ABBREVIATIONS

(TEM) transmission electron microscopy; (E-TEM) environmental TEM; (XPS) X-ray photoemission spectroscopy; (EELS) electron energy loss spectroscopy

REFERENCES

(1) Schmid, M.; Leonardelli, G.; Tscheliessnig, R.; Biedermann, A.; Varga, P. Oxygen adsorption on Al(111): low transient mobility. *Surf. Sci.* **2001**, *478*, L355−L362.

(2) Brune, H.; Wintterlin, J.; Trost, J.; Ertl, G.; Wiechers, J.; Behm, R. J. Interaction of oxygen with Al(111) studied by scanning tunneling microscopy. *J. Chem. Phys.* **1993**, *99*, 2128−2148.

(3) Cai, N.; Zhou, G.; Müller, K.; Starr, D. E. Tuning the Limiting Thickness of a Thin Oxide Layer on Al(111) with Oxygen Gas Pressure. *Phys. Rev. Lett.* **2011**, *107*, 035502.

(4) Jeurgens, L. P. H.; Sloof, W. G.; Tichelaar, F. D.; Mittemeijer, E. J. Growth kinetics and mechanisms of aluminum-oxide films formed by thermal oxidation of aluminum. *J. Appl. Phys.* **2002**, *92*, 1649−1656.

(5) Snijders, P. C.; Jeurgens, L. P. H.; Sloof, W. G. Structure of thin aluminium-oxide films determined from valence band spectra measured using XPS. *Surf. Sci.* **2002**, *496*, 97−109.

(6) Braaten, O.; Kjekshus, A.; Kvande, H. The possible reduction of alumina to aluminum using hydrogen. *JOM* **2000**, *52*, 47−53.

(7) Takeda, S.; Kuwauchi, Y.; Yoshida, H. Environmental transmission electron microscopy for catalyst materials using a spherical aberration corrector. *Ultramicroscopy* **2015**, *151*, 178−190.

(8) Jeurgens, L. P. H.; Sloof, W. G.; Tichelaar, F. D.; Mittemeijer, E. J. Thermodynamic stability of amorphous oxide films on metals: Application to aluminum oxide films on aluminum substrates. *Phys. Rev. B: Condens. Matter Mater. Phys.* **2000**, *62*, 4707−4719.

(9) Greiner, M. T.; Jones, T. E.; Johnson, B. E.; Rocha, T. C. R.; Wang, Z. J.; Armbruster, M.; Willinger, M.; Knop-Gericke, A.; Schlogl, R. The oxidation of copper catalysts during ethylene epoxidation. *Phys. Chem. Chem. Phys.* **2015**, *17*, 25073−25089.

(10) Zou, L.; Li, J.; Zakharov, D.; Stach, E. A.; Zhou, G. In situ atomic-scale imaging of the metal/oxide interfacial transformation. *Nat. Commun.* **2017**, *8*, 307.

(11) Farra, R.; Cao, J.; Rinaldi, A.; Wang, Z.-J.; Kudrenko, E.; Huang, X.; Greiner, M.; Schlogl, R.; Willinger, M.-G. Multi-Scale Red-Ox Dynamics of Active Metal Catalysts Revealed by a Combination of In Situ Scanning and Transmission Electron Microscopy. *Microsc. Microanal.* **2017**, *23*, 922−923.

(12) Cao, J.; Cao, J.; Rinaldi, A.; Wang, Z.-J.; Weinberg, G.; Willinger, M.; Schlögl, R. Structural dynamics of copper and nickel substrates during redox reactions studied by in-situ SEM. In *European Microscopy Congress 2016: Proceedings*; Wiley−VCH: Weinheim, Germany, 2016.

(13) Jiang, N.; Spence, J. C. H. On the dose-rate threshold of beam damage in TEM. *Ultramicroscopy* **2012**, *113*, 77−82.

(14) Jiang, N. Electron beam damage in oxides: a review. *Rep. Prog. Phys.* **2016**, *79*, 016501.

(15) Berger, S. D.; Salisbury, I. G.; Milne, R. H.; Imeson, D.; Humphreys, C. J. Electron energy-loss spectroscopy studies of nanometre-scale structures in alumina produced by intense electron-beam irradiation. *Philos. Mag. B* **1987**, *55*, 341−358.

(16) Egerton, R. F.; Li, P.; Malac, M. Radiation damage in the TEM and SEM. *Micron* **2004**, *35*, 399−409.

(17) Luo, L.; Zou, L.; Schreiber, D. K.; Olszta, M. J.; Baer, D. R.; Bruemmer, S. M.; Zhou, G.; Wang, C.-M. In situ atomic scale visualization of surface kinetics driven dynamics of oxide growth on a Ni-Cr surface. *Chem. Commun.* **2016**, *52*, 3300−3303.

(18) Zhou, G.; Luo, L.; Li, L.; Ciston, J.; Stach, E. A.; Saidi, W. A.; Yang, J. C. In situ atomic-scale visualization of oxide islanding during oxidation of Cu surfaces. *Chem. Commun.* **2013**, *49*, 10862−10864.

(19) Zhou, G.; Luo, L.; Li, L.; Ciston, J.; Stach, E. A.; Yang, J. C. Step-Edge-Induced Oxide Growth During the Oxidation of Cu Surfaces. *Phys. Rev. Lett.* **2012**, *109*, 235502.

(20) Jeurgens, L. P. H.; Sloof, W. G.; Tichelaar, F. D.; Mittemeijer, E. J. Structure and morphology of aluminium-oxide films formed by thermal oxidation of aluminium. *Thin Solid Films* **2002**, *418*, 89−101.

(21) Cabrera, N.; Mott, N. F. Theory of the Oxidation of Metals. *Rep. Prog. Phys.* **1949**, *12*, 163−184.

(22) Evertsson, J.; Bertram, F.; Zhang, F.; Rullik, L.; Merte, L. R.; Shipilin, M.; Soldemo, M.; Ahmadi, S.; Vinogradov, N.; Carlà, F.; Weissenrieder, J.; Göthelid, M.; Pan, J.; Mikkelsen, A.; Nilsson, J. O.; Lundgren, E. The thickness of native oxides on aluminum alloys and single crystals. *Appl. Surf. Sci.* **2015**, *349*, 826−832.

(23) Snijders, P. C.; Jeurgens, L. P. H.; Sloof, W. G. Structural ordering of ultra-thin, amorphous aluminium-oxide films. *Surf. Sci.* **2005**, *589*, 98−105.

(24) Samain, L.; Jaworski, A.; Edén, M.; Ladd, D. M.; Seo, D.-K.; Javier Garcia-Garcia, F.; Häussermann, U. Structural analysis of highly porous γ-Al2O3. *J. Solid State Chem.* **2014**, *217*, 1−8.

(25) Smrcok, L.; Langer, V.; Krestan, J. [gamma]-Alumina: a single-crystal X-ray diffraction study. *Acta Crystallogr., Sect. C: Cryst. Struct. Commun.* **2006**, *62*, i83−i84.

(26) Flototto, D.; Wang, Z. M.; Jeurgens, L. P. H.; Mittemeijer, E. J. Intrinsic stress evolution during amorphous oxide film growth on Al surfaces. *Appl. Phys. Lett.* **2014**, *104*, 091901.

(27) Myers, G. E.; Montet, G. L. Light-induced oxidation of $NbSe_2$ single crystals. *J. Phys. Chem. Solids* **1971**, *32*, 2645.

(28) Cai, N.; Zhou, G.; Müller, K.; Starr, D. E. Effect of oxygen gas pressure on the kinetics of alumina film growth during the oxidation of Al(111) at room temperature. *Phys. Rev. B: Condens. Matter Mater. Phys.* **2011**, *84*, 125445.

(29) Cai, N.; Zhou, G.; Müller, K.; Starr, D. E. Temperature and pressure dependent Mott potentials and their influence on self-limiting oxide film growth. *Appl. Phys. Lett.* **2012**, *101*, 171605.

(30) Popova, I.; Zhukov, V.; Yates, J. T. Electrostatic field enhancement of Al(111) oxidation. *Phys. Rev. Lett.* **2002**, *89*, 276101.

(31) Zhukov, V.; Popova, I.; Yates, J. T. Electron-stimulated oxidation of Al(111) by oxygen at low temperatures: Mechanism of enhanced oxidation kinetics. *Phys. Rev. B: Condens. Matter Mater. Phys.* **2002**, *65*, 195409.

(32) García Ferré, F.; Mairov, A.; Ceseracciu, L.; Serruys, Y.; Trocellier, P.; Baumier, C.; Kaïtasov, O.; Brescia, R.; Gastaldi, D.; Vena, P.; Beghi, M. G.; Beck, L.; Sridharan, K.; Di Fonzo, F. *Sci. Rep.* **2016**, *6*, 33478.

(33) Nakamura, R.; Ishimaru, M.; Yasuda, H.; Nakajima, H. Atomic rearrangements in amorphous Al_2O_3 under electron-beam irradiation. *J. Appl. Phys.* **2013**, *113*, 064312.

DOI: 10.1021/acsami.7b17224
ACS Appl. Mater. Interfaces 2018, 10, 2230−2235